

## Wavelength modulated absorption spectra of Cu<sub>2</sub>O thin films sandwiched by MgO plates

Kazunori IWAMITSU<sup>1</sup>, Shingo AIHARA<sup>1</sup>, Akinobu OTA<sup>2</sup>, Yusuke YOSHIKAZI<sup>1</sup>  
Tomoshige SHIMAMOTO<sup>3</sup>, Atsuhiko FUJII<sup>3</sup> and Ichiro AKAI<sup>3</sup>

<sup>1)</sup> *Graduate School of Science and Technology, Kumamoto University,*

<sup>2)</sup> *Faculty of Science, Kumamoto University,*

<sup>3)</sup> *Shockwave and Condensed Matter Research Center, Kumamoto University,  
2-39-1, Kurokami Chuo-ku, Kumamoto, 860-8555, Japan*

(Received November 30, 2012)

We investigated temperature dependence of wavelength modulated (WM) absorption spectra for studying stress effects on a Cu<sub>2</sub>O thin film. In these spectra, 2P~4P spectral structures can be clearly detected in both yellow and green excitons even at 180 K. From temperature dependences of these resonance energy, one can find that, because of a difference in the thermal variation of the lattice constant between Cu<sub>2</sub>O and MgO, the band gap energies of these excitons systems in the thin film vary in different behaviors from those in Cu<sub>2</sub>O bulk crystals. By comparing our experimental results and Trebin's model, it is understood that this difference is caused by a symmetrical difference of the valence bands between the yellow ( $\Gamma_7^+$ ) and green ( $\Gamma_8^+$ ) exciton systems in Cu<sub>2</sub>O.

### §1. Introduction

Para-excitons in Cu<sub>2</sub>O have attracted much interest because 1S para-excitons have great feasibility to realize excitonic Bose-Einstein condensation (BEC) in high density regime.<sup>1)</sup> Recently, K. Yoshioka *et al.*<sup>2)</sup> have revealed that the formation of a shallow potential is the necessity for the attainment of the excitonic BEC in Cu<sub>2</sub>O in order to suppress inelastic scatterings among high density excitons.<sup>2)</sup> Uniaxial stresses on Cu<sub>2</sub>O crystals are useful to trap the para-excitons, because a certain uniaxial stress shifts their resonance energies to lower energy side in the 1S yellow excitonic series.<sup>3)</sup>

In our study, we employ Cu<sub>2</sub>O thin films sandwiched by MgO plates in order to investigate the uniaxial stress effects on Cu<sub>2</sub>O. In such films, a lattice mismatch between Cu<sub>2</sub>O and MgO is expected to cause compressive stresses to Cu<sub>2</sub>O thin films near hetero-interfaces. On the other hand, it is well known that the yellow exciton state consists of a valence band with a symmetry  $\Gamma_7^+$  different from that of the green exciton state ( $\Gamma_8^+$ ). Therefore, the compressive stresses in the Cu<sub>2</sub>O thin films are expected to have different effects on these valence bands ( $\Gamma_7^+$  and  $\Gamma_8^+$ ). In our paper, we study temperature dependences of band gap energies in the yellow and green excitons of Cu<sub>2</sub>O thin films and focus on the energy shift of their band gap energies in the Cu<sub>2</sub>O thin films from bulk crystals for clarifying the compressive stress effects in the Cu<sub>2</sub>O thin films.

## §2. Experimental



Fig. 1. A photograph of a  $\text{Cu}_2\text{O}$  thin film sandwiched by MgO plates. The dimensions of the sample are  $5 \times 10 \times 1 \text{ mm}^3$ . The thickness of the  $\text{Cu}_2\text{O}$  thin film is  $1.3 \sim 4.3 \text{ }\mu\text{m}$ .<sup>5)</sup>

Figure 1 shows a photograph of a  $\text{Cu}_2\text{O}$  thin film sandwiched by MgO plates. The thin film was fabricated in a small gap between paired MgO plates by melting and re-crystallization from  $\text{Cu}_2\text{O}$  powder.<sup>4)</sup> By heating to higher temperature than the melting point of  $\text{Cu}_2\text{O}$  (1508 K), which is lower than that of MgO, the  $\text{Cu}_2\text{O}$  powder melts and percolates into the small gap by capillary force. The lattice constants of  $\text{Cu}_2\text{O}$  and MgO are 4.2696 and 4.2126 Å at room temperature, respectively. Since a lattice mismatch of  $\text{Cu}_2\text{O}$  and MgO is small (+1.34 %), the  $\text{Cu}_2\text{O}$  thin film is re-crystallized epitaxially on the MgO (100) surface.<sup>4)</sup> By comparing an absorption intensity of the thin film and an absorption coefficient of the  $\text{Cu}_2\text{O}$  bulk crystal at 7.5 K,<sup>5)</sup> the thickness of the  $\text{Cu}_2\text{O}$  thin film (Fig. 1) is estimated to be  $1.3 \sim 4.3 \text{ }\mu\text{m}$ .

As far as we use an ordinary absorption measuring system, it is difficult to analyze spectral structures of the excitonic resonances because of their much weak absorption intensities. We utilized a wavelength modulation (WM) system for highly sensitive absorption spectroscopy in order to observe fine structures of the excitonic resonances. Figure 2 shows a schematic diagram of our WM absorption system. In this system,<sup>6)</sup> an output mirror in a monochromator was yawed slightly for the WM by a resonating vibration unit (WM unit) in Fig. 2.

As shown in Fig. 2, the reference light intensity  $I_0(\lambda)$  passing through the monochromator was recorded by a picoammeter. By yawing of the output mirror with a WM frequency  $f$ , the light intensity  $I(\lambda, t)$  transmitted through the sample is expressed by Eqn. (2.1).

$$I(\lambda, t) = I_0^C(\lambda) - \Delta I(\lambda) \sin(2\pi ft + \delta). \quad (2.1)$$

In this equation,  $I_0^C(\lambda)$  is a transmitted light intensity without WM. On the other hand,  $\Delta I(\lambda)$  was measured as a WM signal by a lock-in amplifier with the frequency  $f$ , and can be written as Eqn. (2.2) under a small amplitude condition ( $\Delta\lambda \ll \lambda$ ),

$$\Delta I(\lambda) \equiv \left( \frac{dI}{d\lambda} \right) \Delta\lambda, \quad (2.2)$$

where  $\Delta\lambda$  is a WM amplitude.

From Eqns. (2.1) and (2.2), one can obtain a wavelength derivative of an absorption coefficient  $\alpha(\lambda)$  as follows:

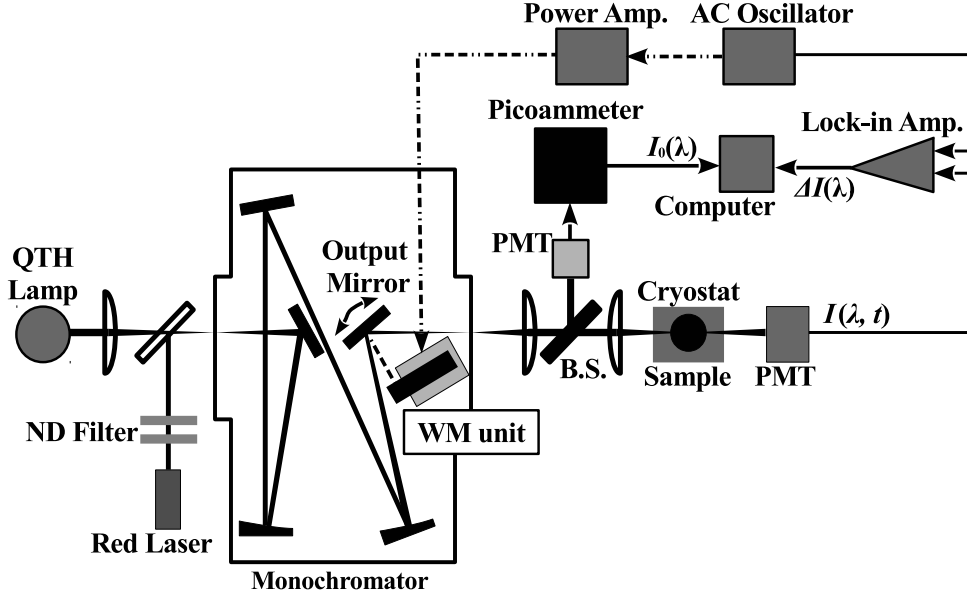


Fig. 2. A schematic diagram of a wavelength modulation (WM) system for high sensitivity absorption spectroscopy. A light source is a quartz tungsten halogen (QTH) lamp. In our system, the wavelength modulation is realized by yawing an output mirror in a monochromator. The transmitted light intensity through a sample is measured by a lock-in amplifier to detect WM absorption signals.

$$\frac{d\alpha(\lambda)}{d\lambda} = \frac{1}{x\Delta\lambda} \frac{\Delta I(\lambda)}{I_0^C(\lambda)}, \quad (2.3)$$

where  $x$  is a sample thickness. In our measurements, the WM amplitude was adjusted to be 3.2 nm.

### §3. Results

#### 3.1. WM absorption spectra

Figures 3-(a) and -(b) show an ordinary and a WM absorption spectrum of the  $\text{Cu}_2\text{O}$  thin film, respectively. In Fig. 3-(a), one can identify 2P and 3P resonance peaks of yellow excitons<sup>7)</sup> in 2.14~2.17 eV and those of green excitons<sup>8)</sup> in 2.25~2.29 eV. On the other hand, 2P~4P dispersive spectral structures of the yellow and green excitons can be clearly confirmed in these WM absorption spectra depicted in Fig. 3-(b).

As described in Sec. 2, a lattice mismatch arises in the  $\text{Cu}_2\text{O}$  thin film owing to a difference of lattice constants between  $\text{MgO}$  ( $a_{\text{MgO}}$ ) and  $\text{Cu}_2\text{O}$  ( $a_{\text{Cu}_2\text{O}}$ ). In addition, due to a difference of thermal variations between  $a_{\text{MgO}}$ <sup>9)</sup> and  $a_{\text{Cu}_2\text{O}}$ <sup>10)</sup>, the lattice mismatch becomes obvious with cooling down. Therefore, we investigated temperature dependence of the WM absorption spectrum in the  $\text{Cu}_2\text{O}$  thin film to

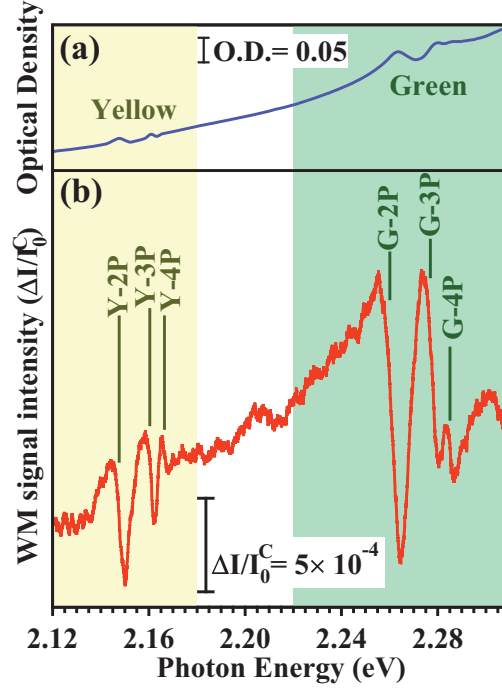


Fig. 3. An ordinary (a) and a WM (b) absorption spectrum of the  $\text{Cu}_2\text{O}$  thin film, respectively. The ordinate is for optical density (a) and a WM signal intensity  $\Delta I/I_0^C$  (b), respectively.

clarify the compressive stress effects on the yellow and green excitons.

Figures 4-(a) and (b) indicate thermal variations of WM absorption spectra in the yellow and green excitons of the  $\text{Cu}_2\text{O}$  thin film, respectively, in which the ordinates are WM signal intensities  $\Delta I/I_0$  and the ordinates above 120 K are magnified to 2.5 times compared to those below 90 K. In Fig. 4, it is found that the 2P~4P yellow- and green-excitonic resonance structures shift to low energy side with elevating temperature.

### 3.2. Temperature dependences of band gap energies

In order to investigate the compressive stress effects in the  $\text{Cu}_2\text{O}$  thin film, we need to evaluate the band gap energy  $E_g$  of the yellow and green excitons from Fig. 4. Down arrows in Fig. 4 indicate the central energies between the maximum and the minimum of dispersive spectral structures by 2P~4P excitonic resonances. In  $\text{Cu}_2\text{O}$ , the excitonic resonance energy  $E_n(T)$  with a quantum number  $n$  can be written by

$$E_n(T) = E_g(T) - \frac{R_y^*}{n^2}, \quad (3.1)$$

where  $E_g(T)$  and  $R_y^*$  are the band gap energy and the effective Rydberg constant, respectively. From the 2P~4P excitonic resonance energies (Fig. 4), we obtained the band gap energies in the yellow and green excitons of the  $\text{Cu}_2\text{O}$  thin film by using Eqn. (3.1). Open circles in Fig. 5-(a) and -(b) show temperature dependences of the band gap energies in the green and yellow excitons, respectively. On the other

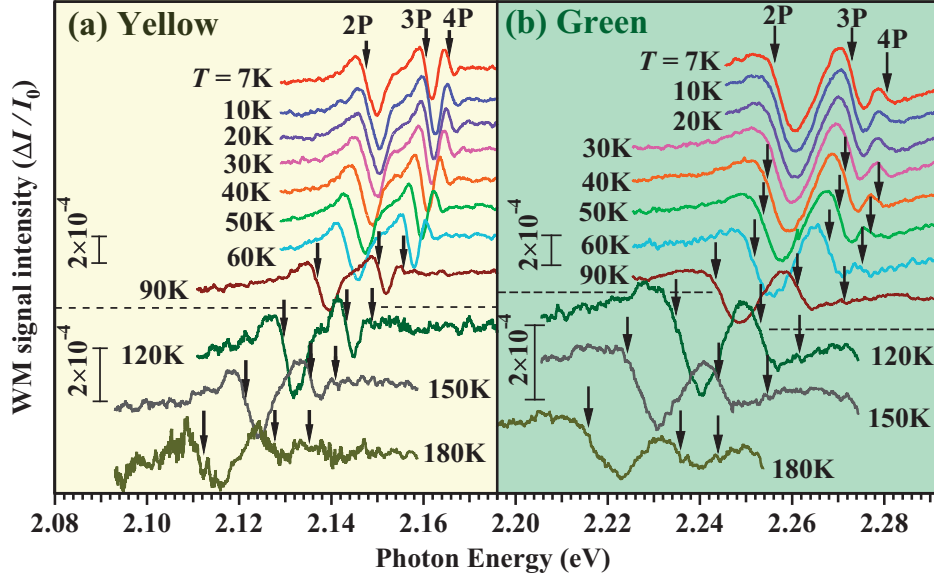


Fig. 4. Thermal variations ( $T = 7 \sim 180$  K) of WM absorption spectra in the yellow (a) and green (b) excitons of the  $\text{Cu}_2\text{O}$  thin film sandwiched by MgO plates.

hand, the thermal variations of the band gap energies have been clarified well in the  $\text{Cu}_2\text{O}$  bulk crystal. According to a previous work,<sup>11)</sup> the band gap energies for the yellow ( $E_g^{(Y)}$ ) and the green ( $E_g^{(G)}$ ) excitons can be expressed by Eqns. (3.2) and (3.3), respectively.

$$E_g^{(Y)}(T) = 2.1984 - 0.0257 \coth\left(\frac{\hbar\omega}{2k_B T}\right) \text{ eV}, \quad (3.2)$$

$$E_g^{(G)}(T) = 2.3304 - 0.0281 \coth\left(\frac{\hbar\omega}{2k_B T}\right) \text{ eV}. \quad (3.3)$$

In Figs. 5-(a) and (b), broken lines denote the  $E_g^{(Y)}(T)$  and  $E_g^{(G)}(T)$  as functions of temperature. In Eqns. (3.2) and (3.3),  $\hbar\omega$  is the energy of  $\Gamma_{12}^-$  optical phonon (13.6 meV).

One can find that the open circles deviate obviously in Fig. 5-(a) and slightly in Fig. 5-(b) from the respective broken lines. Figure 5-(c) shows temperature dependences of the energy shifts of the band gap energies in the thin film from the Eqns. (3.2) and (3.3) in the bulk crystal. At low temperatures, it is found that the red-shift of the green exciton is much larger than that of the yellow exciton in the  $\text{Cu}_2\text{O}$  thin film in Fig. 5-(c).

#### §4. Discussion

In  $\text{Cu}_2\text{O}$ , the yellow and green exciton systems consist of different valence bands having different symmetries ( $\Gamma_7^+$  and  $\Gamma_8^+$ ).<sup>13)</sup> In this section, we take it into account

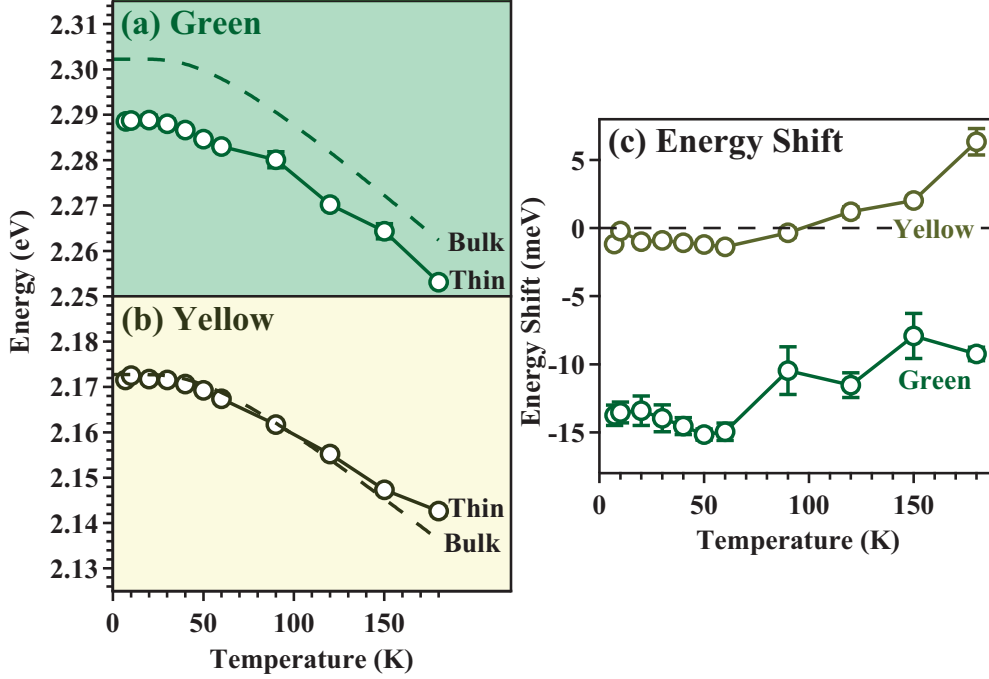


Fig. 5. (a), (b) Temperature dependences of band gap energies in the green (a) and yellow (b) exciton systems. In both figures, open circles and broken lines denote temperature dependences of band gap energies in the thin film and the bulk crystal, respectively. (c) Temperature dependences of the energy shifts of the yellow and green excitons in the  $\text{Cu}_2\text{O}$  thin film.

for understanding the different behaviors of the red-shifts (Fig. 5-(c)) between the yellow and green exciton systems and discuss a difference of compressive stress effects on their exciton systems in the  $\text{Cu}_2\text{O}$  thin film.

#### 4.1. Symmetries of the conduction and valence bands

Figure 6-(a) shows symmetries of the conduction and valence bands in the  $\text{Cu}_2\text{O}$  crystal. The conduction band consists of a hybrid orbit of 4s in Copper atoms and 3s in Oxygen atoms, which has a  $\Gamma_1^+$  symmetry. On the other hand, although the valence band is based on a 3d orbit in Copper atoms, owing to a crystal field of a  $\text{O}_h$  symmetry in the  $\text{Cu}_2\text{O}$  crystal, the valence band splits into twofold  $\Gamma_3^+$  ( $E_g$ ) and threefold  $\Gamma_5^+$  ( $T_{2g}$ ) bands, in which the  $\Gamma_5^+$  band is located at a higher energy side than the  $\Gamma_3^+$  band. The conduction and valence bands for the yellow and green exciton systems are constructed in consideration of spin-orbit interactions ( $\Gamma_6^+$ ) on the  $\Gamma_1^+$  (conduction) and  $\Gamma_5^+$  (valence) bands.<sup>12)</sup> As a consequence, the conduction band has a  $\Gamma_6^+$  symmetry and the  $\Gamma_5^+$  valence band splits into two bands  $\Gamma_7^+$  and  $\Gamma_8^+$  as shown in Fig. 6-(a), where the splitting energy is about 0.13 eV and the degeneracies of the higher lying  $\Gamma_7^+$  and the lower lying  $\Gamma_8^+$  valence bands are twofold and fourfold, respectively. Therefore, the yellow and green excitons consist of the valence band having the different symmetries  $\Gamma_7^+$  and  $\Gamma_8^+$ , respectively.<sup>8)</sup> Figure 6-(b)

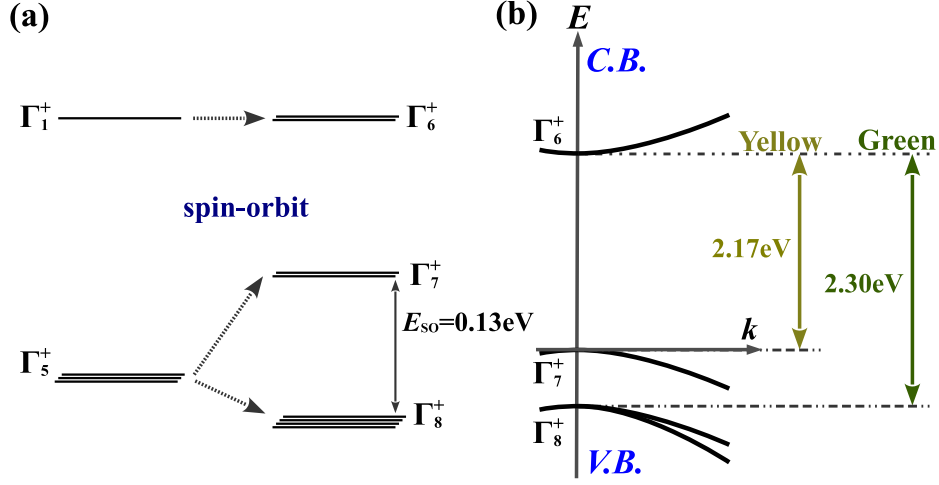


Fig. 6. (a) A schematic diagram of symmetries of the conduction and valence bands in the  $\text{Cu}_2\text{O}$  crystal. (b) A band structure of the  $\text{Cu}_2\text{O}$  crystal in the vicinity of  $\Gamma$  point.

shows the band structure in the vicinity of the  $\Gamma$  point ( $\mathbf{k}=\mathbf{0}$ ) in the  $\text{Cu}_2\text{O}$  crystal. A wavefunction of an excitonic state is written by the product of an envelope function, which describes electron-hole relative motion and a hole in the exciton state and both Bloch wavefunctions of the electron (conduction band) and of the hole (valence band). In the case of the yellow and green excitons in the  $\text{Cu}_2\text{O}$  crystal, their wavefunctions have different symmetries owing to the Bloch wavefunctions of the hole in the different valence bands ( $\Gamma_8^+$  and  $\Gamma_7^+$ ). Therefore, it is expected that the compressive stress affects the yellow and green excitonic states in a different way.

#### 4.2. Uniaxial stress effects of the yellow and green excitons

H.-R. Trebin *et al.*<sup>14</sup> demonstrated that the yellow and green exciton states are strongly mixed by a uniaxial stress in the  $\text{Cu}_2\text{O}$  crystal and studied energy changes of the excitonic states. Since we take into account of the mixing between the yellow and green exciton states according to Trebin's theory, we begin to consider the  $\Gamma_5^+$  valence band before spin-orbit splitting (Fig. 6-(a)).<sup>14</sup> For studying the uniaxial stress effect, they introduced an effective Hamiltonian  $\mathcal{H}_x$  as follows:

$$\mathcal{H}_x = \mathcal{H}_0 + \mathcal{H}_{\text{ex}} + \mathcal{H}_d. \quad (4.1)$$

In this equation,  $\mathcal{H}_0$  is an unperturbed Hamiltonian and we use its eigenfunctions for wavefunctions of the excitonic states. The second and third terms in Eqn. (4.1) mean an exchange interaction and a perturbation due to the uniaxial stress. For the Hamiltonian  $\mathcal{H}_x$ , they employed linear combinations of the basis wavefunctions as written in Eqn. (4.2)<sup>14</sup> for describing the yellow and green exciton states under uniaxial stress.

$$\Psi_x = \sum f_{LJFG_z}(r) |LJFG_z\rangle, \quad (4.2)$$

where  $\mathbf{F} \equiv \mathbf{L} + \mathbf{J}$ ,  $\mathbf{L} = \mathbf{r} \times \mathbf{p}$ ,  $\mathbf{J} \equiv \mathbf{I} + (1/2)\boldsymbol{\sigma}^h$ ,  $\mathbf{G} \equiv \mathbf{F} + (1/2)\boldsymbol{\sigma}^e$ ,  $\mathbf{I}$  is the angular momentum matrix and  $\boldsymbol{\sigma}^h$  and  $\boldsymbol{\sigma}^e$  are the Pauli matrices of holes and

electrons, respectively. Without the perturbation of  $\mathcal{H}_d$ , the yellow- and green-excitonic wavefunctions can be expressed in Eqns. (4.3) and (4.4), respectively.<sup>14)</sup>

$$|yGG_z\rangle = f_{0\frac{1}{2}\frac{1}{2}GG_z}(r) \left| 0\frac{1}{2}\frac{1}{2}GG_z \right\rangle + f_{2\frac{3}{2}\frac{1}{2}GG_z}(r) \left| 2\frac{3}{2}\frac{1}{2}GG_z \right\rangle, \quad (4.3)$$

$$|gGG_z\rangle = f_{0\frac{3}{2}\frac{3}{2}GG_z}(r) \left| 0\frac{3}{2}\frac{3}{2}GG_z \right\rangle + f_{2\frac{3}{2}\frac{3}{2}GG_z}(r) \left| 2\frac{3}{2}\frac{3}{2}GG_z \right\rangle + f_{2\frac{1}{2}\frac{3}{2}GG_z}(r) \left| 2\frac{1}{2}\frac{3}{2}GG_z \right\rangle, \quad (4.4)$$

where  $f_{LJFG_z}(r)$  are mixing coefficients of the basis functions  $|LJFG_z\rangle$ . In the Trebin's expression of Eqns. (4.3) and (4.4), the 2S yellow para-exciton state is described as a mixed state of 98% yellow S-type ( $L = 0, J = 1/2, F = 1/2$ ) and 2% green D-type ( $L = 2, J = 3/2, F = 1/2$ ) states. On the other hand, the 1S green para-exciton state is expressed as a mixed state of 80% green S-type ( $L = 0, J = 3/2, F = 3/2$ ), 2% green D-type ( $L = 2, J = 3/2, F = 3/2$ ) and 18% yellow D-type ( $L = 2, J = 1/2, F = 3/2$ ) states. By using these wavefunctions as basis functions, one can obtain matrix elements of  $\mathcal{H}_x$ . For instance, the matrix of  $\mathcal{H}_x$  for the yellow and green ortho-exciton states  $|y10\rangle$  and  $|g10\rangle$  ( $G = 1, G_z = 0$ ) can be written in Eqns. (4.5) and (4.6) for the basis wavefunctions of the ortho-excitons ( $G = 1, G_z = 0$ ) in the yellow  $|y10\rangle$  and green  $|g10\rangle$  exciton systems.

$$\begin{pmatrix} E(y) + hX - \frac{2}{3}J_y & \frac{2\sqrt{2}}{3}J - e\sqrt{2}X \\ \frac{2\sqrt{2}}{3}J - e\sqrt{2}X & E(g) + hX + dX - \frac{4}{3}J_g \end{pmatrix}, \quad (4.5)$$

$$J \equiv -\frac{c}{4\pi} f_{0\frac{1}{2}\frac{1}{2}GG_z}(0) f_{0\frac{3}{2}\frac{3}{2}GG_z}(0), \quad J_y \equiv -\frac{c}{4\pi} f_{0\frac{1}{2}\frac{1}{2}GG_z}^2(0),$$

$$J_g \equiv -\frac{c}{4\pi} f_{0\frac{3}{2}\frac{3}{2}GG_z}^2(0), \quad c \equiv \frac{C}{Ra^3}, \quad C = \sum_{\mathbf{K} \neq \mathbf{0}} \frac{\langle \Gamma_1^+ | e^{i\mathbf{K} \cdot \mathbf{r}} | \Gamma_5^+ \rangle}{K^2}. \quad (4.6)$$

where  $E(y)$  and  $E(g)$  indicate the eigenvalues of the  $\mathcal{H}_0$  for the basis wavefunctions of the yellow- and green-exciton states and  $h, e$  and  $d$  are parameters characterizing the uniaxial strain  $X$ , respectively.

As summarized in Sec. 4.1, the valence bands  $\Gamma_7^+$  and  $\Gamma_8^+$  degenerate in twofold and fourfold, respectively. On the other hand, the conduction band having a  $\Gamma_6^+$  symmetry also degenerates in twofold as shown in Fig. 6-(a). On the basis of the electron and hole states in these bands, five kinds of excitonic states are constructed through exchange interactions among them. As a result, threefold  $\Gamma_5^+$  ortho-exciton and a single  $\Gamma_2^+$  para-exciton states are formed in the yellow exciton system from the  $\Gamma_6^+$  conduction (twofold) and the  $\Gamma_7^+$  valence (twofold) bands. On the other hand, in the green exciton system, threefold  $\Gamma_4^+$  excitons and twofold  $\Gamma_3^+$  excitons as well as threefold  $\Gamma_5^+$  ortho-exciton states are formed from the same conduction ( $\Gamma_6^+$ : twofold) and the  $\Gamma_8^+$  valence (fourfold) bands. Now, it should be noted that the ortho-exciton states in both excitonic systems degenerate in threefold without uniaxial stress.

By using these formalism, H.-R. Trebin *et al.* studied a uniaxial stress effect along [100] direction in the  $\text{Cu}_2\text{O}$  crystal and demonstrated that the threefold ortho-exciton states split into a twofold  $\Pi_g$  state and a single  $\Sigma_g^-$  state due to the uniaxial

stress. They have given expressions of splitting energies  $\Delta E^{(Y,G)}$  ( $= E^{(Y,G)}(\Pi_g) - E^{(Y,G)}(\Sigma_g^-)$ ) between the  $\Pi_g$  and  $\Sigma_g^-$  states in both excitonic systems (Y: yellow, G: green) as functions of the uniaxial strain  $X$ . Equations (4.7) and (4.8) represent their results for the yellow and green ortho-exciton states, respectively.

$$\Delta E^{(Y)} = -\frac{4Je}{\Delta'}X \quad (< 0), \quad (4.7)$$

$$\Delta E^{(G)} = +\frac{4Je}{\Delta'}X - \frac{3}{2}dX - \frac{3e^2}{2}\Delta'X^2 + \frac{9}{16}d^2X^2 \quad (> 0). \quad (4.8)$$

In the case of the compressive stress ( $X < 0$ ) along [100] direction in the  $\text{Cu}_2\text{O}$  crystal, they indicated that the parameters  $J$ ,  $\Delta'$  ( $\equiv E(g) - E(y)$ ),  $e$  and  $d$  have the values of  $J < 0$ ,  $\Delta' > 0$ ,  $e > 0$  and  $d > 0$ , respectively.<sup>14)</sup> In Eqn. (4.7), the  $\Delta E^{(Y)}$  of the yellow ortho-exciton is written only by the product of the exchange interaction strength  $J$  and the uniaxial strain  $X$ . On the other hand, the  $\Delta E^{(G)}$  has a different dependence on the strain  $X$  as seen in Eqn. (4.8), where the third and fourth terms having  $X^2$  dependence are also included.

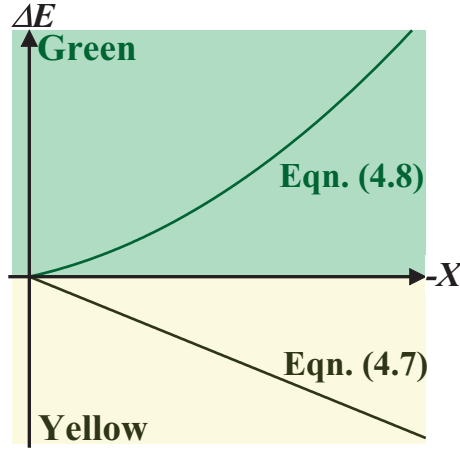


Fig. 7. Stress dependence of the energetic difference after the subtraction of a singlet from a doublet in yellow and green excitonic series.

Figure 7 shows synoptic variations of  $\Delta E^{(Y)}$  (Eqn. (4.7)) and  $\Delta E^{(G)}$  (Eqn. (4.8)) as functions of the uniaxial strain  $X$ . In this figure, one can find that the  $\Delta E^{(Y)}$  has negative values and is proportional to  $X$ . On the other hand, the  $\Delta E^{(G)}$  has a different dependence on the uniaxial strain  $X$  along [100] direction as seen in Fig. 7. Their model can well explain the experimental results by R. G. Waters *et al.* under the uniaxial stress along [100] direction.<sup>13)</sup> In addition, H.-R. Trebin *et al.*<sup>14)</sup> also demonstrated that, under another strain along [110] direction, the uniaxial stress effects are also different between the yellow and green exciton systems reflecting their symmetry difference.

In our sample, the  $\text{Cu}_2\text{O}$  thin film is sandwiched by paired  $\text{MgO}$  plates with [100] surface. The lattice constant of the  $\text{Cu}_2\text{O}$  crystal is slightly larger than that of the

MgO plates as mentioned in Sec. 2. In consequence, it is expected that the  $\text{Cu}_2\text{O}$  thin film undergoes two-dimensional compressive strain along perpendicular directions to the [100] direction on the interface with the MgO plates. In the  $\text{Cu}_2\text{O}$  thin film, we demonstrated that the thermal variation of the energy shifts depending on temperature have different behaviors between the yellow and green exciton systems as shown in Fig. 5. Although more precise analyses are required for a quantitative modeling for explanation of these experimental results, it is considered that such different behaviors come from the symmetry difference between the yellow and green exciton systems in a similar way with the Trebin's model.

## §5. Summary

In order to investigate the formation of an exciton-trapping potential in  $\text{Cu}_2\text{O}$  thin films sandwiched by MgO plates, we examined temperature dependences of the band gap energies of the yellow and green exciton systems in the  $\text{Cu}_2\text{O}$  thin film by measuring thermal variations of the WM absorption spectra. In the WM absorption spectra, we can detect the 2P~4P resonance structures of the yellow and green exciton systems in wide temperature range from 7 K to 180 K. From these results, it is found that, because of a difference between the thermal variations of the lattice constants in  $\text{Cu}_2\text{O}$  and MgO, the band gap energies of these exciton systems in the thin film vary in different behaviors from those in the bulk crystal. In addition, a difference of the exciton-trapping potential depth between the yellow and green excitons is also clarified. At low temperature limit, the red shift of the band gap energy from that of the bulk crystal in the green exciton system is much larger than that in the yellow exciton system. It is qualitatively understood that this difference is caused by the symmetry difference of the valence bands between the yellow ( $\Gamma_7^+$ ) and green ( $\Gamma_8^+$ ) exciton systems.

## Acknowledgements

This work was supported by JSPS KAKENHI No. 22340083 in the Grant-in-Aid for Scientific Research (B).

## References

- 1) S. A. Moskalenko and D. W. Snoke, *"Bose-Einstein Condensation of Excitons and Biexcitons: And Coherent Nonlinear Optics with Excitons"*, Cambridge University Press (2005).
- 2) K. Yoshioka, E. Chae and M. Kuwata-Gonokami, *Nat. Commun.* **2**, 328 (2011).
- 3) N. Naka and N. Nagasawa, *Phys. Rev. B* **70**, 155205 (2004).
- 4) N. Naka, S. Hashimoto, T. Ishihara, *Jpn J. Appl. Phys.* **44**, 5096 (2005).
- 5) N. Naka, Doctor thesis, Department of Physics, Graduate School of Science, The University of Tokyo, November 2002.
- 6) K. Iwamitsu, S. Aihara, T. Shimamoto, A. Fujii, I. Akai, *Rev. Sci. Instrum.* **83**, 073101 (2012).
- 7) P. W. Baumeister, *Phys. Rev.* **121**, 359 (1961).
- 8) E. F. Gross, *Nuovo Cimento Suppl.* **3**, 672 (1956).
- 9) G. K. White and O. L. Anderson, *J. Appl. Phys.* **37**, 430 (1966).
- 10) G. K. White, *J. Phys. C: Solid State Phys.* **11**, 2171 (1978).
- 11) T. Itoh and S. Narita, *J. Phys. Soc. Japan* **39**, 140 (1975).

- 12) R. J. Elliott, Phys. Rev. **124**, 340 (1961).
- 13) R. G. Waters, F. H. Pollak, R. H. Bruce and H. Z. Cummins, Phys. Rev. B **21**, 1665 (1980).
- 14) H.-R. Trebin, H. Z. Cummins, and J. L. Birman, Phys. Rev. B **23**, 597 (1981).
- 15) D. Fröhlich, R. Kenklies, Ch. Uihlein and C. Schwab, Phys. Rev. Lett **43**, 1260 (1979).